

Bayesian Uncertainty Quantification for Low-rank Matrix Completion

Henry Shaowu Yuchi*, Simon Mak[†], Yao Xie*

December 2020

Abstract

We consider the problem of uncertainty quantification (UQ) for an unknown low-rank matrix \mathbf{X} , given a partial and noisy observation of its entries. This quantification of uncertainty is essential for many real-world problems, including image processing, satellite imaging, and seismology, providing a principled framework for validating scientific conclusions and guiding decision-making. However, existing literature has largely focused on the completion (i.e., point estimation) of the matrix \mathbf{X} , with little work on exploring the uncertainty of such estimates. To this end, we propose in this work a new Bayesian modeling framework, called BayeSMG, which parametrizes the unknown \mathbf{X} via its underlying row and column subspaces. This Bayesian subspace parametrization allows for efficient posterior inference on matrix subspaces (which represent interpretable phenomena in many applications), which can then be leveraged for improved matrix recovery. We demonstrate the effectiveness of BayeSMG over existing Bayesian matrix recovery methods in extensive numerical experiments and a seismic sensor network application.

Keywords: hierarchical modeling, manifold sampling, matrix factorization, matrix completion, seismic imaging, uncertainty quantification

*H. Milton Stewart School of Industrial & Systems Engineering, Georgia Institute of Technology

[†]Department of Statistical Science, Duke University

1 Introduction

Low-rank matrices play a vital role in modeling many scientific and engineering problems, including (but not limited to) image processing, satellite imaging, and network analysis. In such applications, however, only a small portion of the desired matrix (which we denote as $\mathbf{X} \in \mathbb{R}^{m_1 \times m_2}$ in this article) can be observed. The reasons for this are two-fold: (i) the cost of observing all matrix entries can be high, requiring expensive computational, experimental, or communication expenditure; (ii) there can be missing observations at individual entries due to sensor malfunction, experimental failure, or unreliable data transmission. The *matrix completion* problem aims to complete the missing entries of the matrix from a partial (and perhaps noisy) observation. Matrix completion has attracted much attention since the seminal works of Candès and Tao (2010), Candès and Recht (2009), and Recht (2011). The theory and methodology behind point estimation are now well-understood for matrix completion, under the assumption that \mathbf{X} is low-rank, with various convex and non-convex optimization algorithms developed for performing this recovery.

However, much of the literature (a detailed review is provided in Section 1.1) has focused on the completion, i.e., *point estimation*, of \mathbf{X} , with little work on exploring the uncertainty of such estimates. In many scientific and engineering applications, such estimates are much more useful when coupled with a measure of uncertainty. The principled characterization and reduction of this uncertainty are known as *uncertainty quantification* (UQ), see, e.g., Smith, 2013. UQ is becoming increasingly important in various applications, providing a principled framework for validating scientific conclusions and guiding decision-making.

In this paper, we address the problem of UQ for the matrix completion problem from a Bayesian perspective. We propose a novel Bayesian modeling framework, called BayeSMG, which quantifies uncertainty in the desired matrix \mathbf{X} via posterior sampling on its underlying subspaces. BayeSMG can be viewed as a hierarchical Bayesian extension of the singular matrix-variate Gaussian (SMG) distribution (hence its name), with hierarchical priors on matrix subspaces. In addition to providing point estimates on \mathbf{X} , the proposed model also yields UQ on \mathbf{X} via an efficient Gibbs sampler on matrix subspaces. By integrating the subspace structure for posterior inference, we show that BayeSMG enjoys improved recovery performance and better interpretability compared with existing Bayesian models in extensive numerical experiments and a real-world seismic sensor network application.

1.1 Existing literature

Much of the existing literature on inferring \mathbf{X} from partial observations falls under the topic of *matrix completion* – the completion (or point estimation) of \mathbf{X} from observed entries. Early works in this area include the seminal works of Candès and Tao (2010), Candès and Recht (2009), and Recht (2011), which established conditions for exact completion via nuclear-norm minimization, under the assumption that observations are uniformly sampled without noise. This is then extended to the *noisy* matrix completion setting, where entries are observed with noise; important results include Candès and Plan (2010), Keshavan et al. (2010), Koltchinskii et al. (2011), and Negahban and Wainwright (2012), among others. There is now a rich body of work on matrix completion; some recent overviews include Davenport and Romberg (2016); Chi et al. (2019). However, completion focuses solely on the point estimation of the matrix \mathbf{X} and provides no quantification of uncertainty on each unobserved entry. In problems with only a few observed entries (see motivating applications), this uncertainty can be as valuable as the point estimate itself in assessing the quality of the recovery and guiding decision-making.

The aforementioned matrix completion works largely focus on providing point estimators on missing entries for matrix recovery. The problem of quantifying uncertainties in such estimates has been relatively unexplored in the literature, but clearly, an important one given the motivating applications. One recent pioneering work on this is Chen et al. (2019), who proposed entrywise confidence intervals for both convex and non-convex estimators on \mathbf{X} , via debiasing using low-rank factors of the matrix. The resulting debiased estimators admit nearly precise nonasymptotic distributional characterizations, which in turn enable optimal construction of confidence intervals for missing matrix entries and low-rank factors. Our approach has several distinctions from this work: the latter is a frequentist approach with appealing theoretical guarantees, whereas our Bayesian approach instead yields a richer quantification of uncertainty on \mathbf{X} via a hierarchical model.

Another approach for quantifying uncertainty is via Bayesian modeling. There is a growing literature on Bayesian matrix completion, of which the most popular approach is the Bayesian Probabilistic Matrix Factorization (BPMF) method in Salakhutdinov and Mnih (2008). BPMF adopts the following probabilistic model on \mathbf{X} : $\mathbf{X} = \mathbf{M}\mathbf{N}^T$, $\mathbf{M} \in \mathbb{R}^{m_1 \times R}$, $\mathbf{N} \in \mathbb{R}^{m_2 \times R}$, where $R < m_1 \wedge m_2 := \min(m_1, m_2)$ is an upper bound on matrix rank. Each row of the factorized

matrices \mathbf{M} and \mathbf{N} are then assigned i.i.d. Gaussian priors $\mathcal{N}(\boldsymbol{\mu}_M, \Sigma_M)$ and $\mathcal{N}(\boldsymbol{\mu}_N, \Sigma_N)$, respectively, with conjugate normal hyperpriors on row and column means: $\boldsymbol{\mu}_m \sim \mathcal{N}(0, \Sigma_m \beta)$, $\boldsymbol{\mu}_n \sim \mathcal{N}(0, \Sigma_n \beta)$, where $\beta \in \mathbb{R}^{R \times 1}$ is fixed; and Inverse-Wishart hyperpriors on row and column covariance matrices: $\Sigma_m \sim \text{IW}(R, \mathbf{W})$, $\Sigma_n \sim \text{IW}(R, \mathbf{W})$, where \mathbf{W} is a weighted matrix (however, the numerical experiments therein focus on non-informative IW prior). Such a specification allows for an efficient Gibbs sampler, which performs conjugate sampling on each *row* of \mathbf{M} and each *row* of \mathbf{N} , along with conjugate updates on hyper-parameters. This conjugate Gibbs sampler allows the BPFM to tackle problems as large as the Netflix dataset, which has millions of user-movie ratings. Many existing Bayesian matrix completion methods (e.g., Lawrence and Urtasun, 2009; Zhou et al., 2010; Babacan et al., 2011; Alquier et al., 2014) can be viewed as variations or extensions of this BPFM framework.

From a modeling perspective, the key novelty in BayeSMG is that our model requires the involved factorized matrices to be orthonormal (corresponding to the singular value decomposition (SVD) of the matrix \mathbf{X}), whereas the BPFM does not. This provides several key advantages for our method, which we demonstrate later. First, by explicitly parametrizing row and column subspaces as model parameters, BayeSMG can incorporate prior knowledge on subspaces within the prior specification of such parameters. This prior information is often available in many signal processing and image processing problems, e.g., known signal structure or image features. Second, BayeSMG allows for *direct* inference on subspaces of \mathbf{X} via posterior sampling. For subspace inference, our approach avoids performing an additional SVD step for every posterior sample (compared to the BPFM), which significantly speeds up inference for high-dimensional problems (i.e., $m_1 \gg 1$ or $m_2 \gg 1$). Finally (and perhaps most importantly), BayeSMG can leverage this posterior learning on subspaces to provide improved inference for the partially observed matrix \mathbf{X} . Compared to the BPFM, our approach yields faster posterior contraction for unobserved entries when the underlying matrix is low-rank, in both numerical simulations and applications. This allows for a more *accurate* estimate and a more *precise* uncertainty quantification of \mathbf{X} over the BPFM.

The BayeSMG model also provides several novel and interesting theoretical insights. In Section 4, we show that the maximum a posteriori (MAP) estimator takes the form of a regularized matrix estimator, which provides a connection between the proposed method and existing matrix completion techniques. We also show that the BayeSMG model implicitly assumes a probabilistic model on

matrix *coherence* (Candès and Recht, 2009), which measures the “recoverability” of a low-rank matrix. Coherence has been widely used in the matrix completion literature as a theoretical condition for recovery. Through this connection, we then establish an error monotonicity result for BayeSMG, which provides a reassuring check on the UQ performance of the proposed model.

The paper is organized as follows. Section 2 introduces the BayeSMG model. Section 3 presents an efficient posterior sampling algorithm for \mathbf{X} and its subspaces. Section 4 reveals connections between BayeSMG and coherence and its impact on error convergence. Section 5 investigates numerical experiments with synthetic and real data. Section 6 explores a real-world seismic sensor network application. Section 7 concludes with discussions.

2 The BayeSMG model

We first describe the proposed BayeSMG model, which combines the Singular Matrix-variate Gaussian (SMG) distribution with a Bayesian prior specification on matrix subspaces.

2.1 Problem set-up

Let $\mathbf{X} \in \mathbb{R}^{m_1 \times m_2}$ be the matrix of interest, and assume \mathbf{X} is low-rank, i.e., $R := \text{rank}(\mathbf{X}) \ll m_1 \wedge m_2$. Let $[m] := \{1, \dots, m\}$. Suppose \mathbf{X} is sampled with noise at an index set $\Omega \subseteq [m_1] \times [m_2]$ of size $|\Omega| = n$, yielding observations:

$$Y_{i,j} = X_{i,j} + \epsilon_{i,j}, \quad (i,j) \in \Omega. \quad (1)$$

Here, $Y_{i,j}$ is the observation at index (i,j) , corrupted by noise $\epsilon_{i,j}$. In this work, we assume $\epsilon_{i,j} \stackrel{i.i.d.}{\sim} \mathcal{N}(0, \eta^2)$, i.e., noise follows an i.i.d. Gaussian distribution with zero mean and variance η^2 . Further let $\mathbf{Y}_\Omega := (Y_{i,j})_{(i,j) \in \Omega} \in \mathbb{R}^n$ denote the vector of noisy observations, and let \mathbf{X}_{Ω^c} be the vector of unobserved matrix entries, where $\Omega^c := ([m_1] \times [m_2]) \setminus \Omega$ is the set of unobserved indices.

With this framework, the desired goal of uncertainty quantification (UQ) can be made more concrete. Given noisy observations \mathbf{Y}_Ω , we wish to not only estimate the unobserved matrix entries \mathbf{X}_{Ω^c} , but also quantify how *uncertain* for both observed or unobserved entries since there are observation noise.

2.2 SMG model

We adopt the following SMG model for the low-rank matrix \mathbf{X} , assumed to be normalized with zero mean.

Definition 1 (Singular matrix-variate Gaussian (SMG) (Definition 2.4.1, Gupta and Nagar (1999))). *Let $\mathbf{Z} \in \mathbb{R}^{m_1 \times m_2}$ be a random matrix with entries $Z_{i,j} \stackrel{i.i.d.}{\sim} \mathcal{N}(0, \sigma^2)$ for $(i, j) \in [m_1] \times [m_2]$. The random matrix \mathbf{X} has a singular matrix-variate Gaussian (SMG) distribution if $\mathbf{X} \stackrel{d}{=} \mathcal{P}_{\mathcal{U}} \mathbf{Z} \mathcal{P}_{\mathcal{V}}$ for some choice of projection matrices $\mathcal{P}_{\mathcal{U}} = \mathbf{U} \mathbf{U}^T$ and $\mathcal{P}_{\mathcal{V}} = \mathbf{V} \mathbf{V}^T$, where $\mathbf{U} \in \mathbb{R}^{m_1 \times R}$, $\mathbf{U}^T \mathbf{U} = \mathbf{I}$, $\mathbf{V} \in \mathbb{R}^{m_2 \times R}$, $\mathbf{V}^T \mathbf{V} = \mathbf{I}$ and $R < m_1 \wedge m_2$. We will denote this as $\mathbf{X} \sim \text{SMG}(\mathcal{P}_{\mathcal{U}}, \mathcal{P}_{\mathcal{V}}, \sigma^2, R)$.*

In other words, a realization from the SMG distribution can be obtained by first (i) simulating a matrix \mathbf{Z} from a Gaussian ensemble with variance σ^2 (i.e., a matrix with i.i.d. $\mathcal{N}(0, \sigma^2)$ entries), then (ii) performing a left and right projection of \mathbf{Z} using the projection matrices $\mathcal{P}_{\mathcal{U}}$ and $\mathcal{P}_{\mathcal{V}}$. Recall that the projection operator $\mathcal{P}_{\mathcal{U}} = \mathbf{U} \mathbf{U}^T \in \mathbb{R}^{m_1 \times m_1}$ maps a vector in \mathbb{R}^{m_1} to its orthogonal projection on the R -dimensional subspace \mathcal{U} spanned by the columns of \mathbf{U} . By performing this projection, the resulting matrix $\mathbf{X} = \mathcal{P}_{\mathcal{U}} \mathbf{Z} \mathcal{P}_{\mathcal{V}}$ can be shown to be of rank $R < m_1 \wedge m_2$, with its row and column spaces \mathcal{U} and \mathcal{V} corresponding to the subspaces for $\mathcal{P}_{\mathcal{U}}$ and $\mathcal{P}_{\mathcal{V}}$. The matrix \mathbf{X} also lies in the space $\mathcal{T} := \bigcup_{u_k \in \mathcal{U}, v_k \in \mathcal{V}} \text{span}(\{\mathbf{u}_k \mathbf{v}_k^T\}_{k=1}^R)$. With a small choice of R , this distribution provides a flexible model for the low-rank structure of \mathbf{X} .

The SMG distribution provides an appealing probabilistic modeling framework for low-rank matrices. First, the model enables a prior distribution involving the subspaces \mathbf{U} and \mathbf{V} of the matrix \mathbf{X} . Since it is known from Chikuse (2012) that for each projection operator $\mathcal{P} \in \mathbb{R}^{m \times m}$ of rank R , there exists a unique R -dimensional hyperplane (or an R -plane) in \mathbb{R}^m containing the origin which corresponds to the image of such a projection. This connects the space of rank R projection matrices and the *Grassmann manifold* $\mathcal{G}_{R, m-R}$, the space of R -planes in \mathbb{R}^m . Viewed this way, the projection matrices parametrizing $\mathbf{X} \sim \text{SMG}(\mathcal{P}_{\mathcal{U}}, \mathcal{P}_{\mathcal{V}}, \sigma^2, R)$ encode valuable information on the row and column spaces of \mathbf{X} . This allows the incoherence of the matrix to be obtained, which determines whether the recovery of the matrix is possible. For the latent matrix \mathbf{Z} in the SMG model, an entry-wise Gaussian uniform distribution is introduced to ensure the model is not biased. Second, since the projection of a Gaussian random vector is still Gaussian, the left-right projection of the Gaussian ensemble

D results in each entry of \mathbf{X} being Gaussian-distributed as well. This is crucial for deriving useful UQ properties of the BayeSMG model. Finally, we can also control the rank of the matrix approximation by the subspaces.

We now show several distributional properties of the SMG model:

Lemma 2. *Distributional properties of SMG: Let $\mathbf{X} \sim \text{SMG}(\mathcal{P}_U, \mathcal{P}_V, \sigma^2, R)$, with $\mathcal{P}_U \in \mathbb{R}^{m_1 \times m_1}$, $\mathcal{P}_V \in \mathbb{R}^{m_2 \times m_2}$, $\sigma^2 > 0$ and $R < m_1 \wedge m_2$ known. Then:*

1. *The density of \mathbf{X} is given by*

$$f(\mathbf{X}) = (2\pi\sigma^2)^{-R^2/2} \text{etr}\left\{-\frac{1}{2\sigma^2}[(\mathbf{X}\mathcal{P}_V)^T(\mathcal{P}_U\mathbf{X})]\right\}, \quad \mathbf{X} \in \mathcal{T}, \quad (2)$$

where $\text{etr}(\cdot) := \exp\{\text{tr}(\cdot)\}$.

2. *Consider the block decomposition of $\mathcal{P}_V \otimes \mathcal{P}_U$:*

$$\mathcal{P}_V \otimes \mathcal{P}_U = \begin{pmatrix} (\mathcal{P}_V \otimes \mathcal{P}_U)_\Omega & (\mathcal{P}_V \otimes \mathcal{P}_U)_{\Omega, \Omega^c} \\ (\mathcal{P}_V \otimes \mathcal{P}_U)_{\Omega, \Omega^c}^T & (\mathcal{P}_V \otimes \mathcal{P}_U)_{\Omega^c} \end{pmatrix}. \quad (3)$$

Conditional on the observed noisy entries \mathbf{Y}_Ω , the unobserved entries \mathbf{X}_{Ω^c} follow the distribution, $[\mathbf{X}_{\Omega^c} | \mathbf{Y}_\Omega] \sim \mathcal{N}(\mathbf{X}_{\Omega^c}^P, \Sigma_{\Omega^c}^P)$. Here, $\gamma^2 = \eta^2/\sigma^2$, and

$$\begin{aligned} \mathbf{R}_N(\Omega) &:= (\mathcal{P}_V \otimes \mathcal{P}_U)_\Omega \in \mathbb{R}^{N \times N}, \\ \mathbf{X}_{\Omega^c}^P &:= (\mathcal{P}_V \otimes \mathcal{P}_U)_{\Omega, \Omega^c}^T [\mathbf{R}_N(\Omega) + \gamma^2 \mathbf{I}]^{-1} \mathbf{Y}_\Omega, \\ \Sigma_{\Omega^c}^P &:= \sigma^2 \{(\mathcal{P}_V \otimes \mathcal{P}_U)_{\Omega^c} - (\mathcal{P}_V \otimes \mathcal{P}_U)_{\Omega, \Omega^c}^T [\mathbf{R}_N(\Omega) + \gamma^2 \mathbf{I}]^{-1} (\mathcal{P}_V \otimes \mathcal{P}_U)_{\Omega, \Omega^c}^T\}. \end{aligned} \quad (4)$$

3. *Conditional on the observed noisy entries \mathbf{Y}_Ω , the observed entries \mathbf{X}_Ω follow the distribution: $[\mathbf{X}_\Omega | \mathbf{Y}_\Omega] \sim \mathcal{N}(\mathbf{X}_\Omega^P, \Sigma_\Omega^P)$, where $\mathbf{R}_N(\Omega) = (\mathcal{P}_V \otimes \mathcal{P}_U)_\Omega$, and*

$$\begin{aligned} \mathbf{X}_\Omega^P &:= (\mathcal{P}_V \otimes \mathcal{P}_U)_\Omega [\mathbf{R}_N(\Omega) + \gamma^2 \mathbf{I}]^{-1} \mathbf{Y}_\Omega, \\ \Sigma_\Omega^P &:= \sigma^2 \{(\mathcal{P}_V \otimes \mathcal{P}_U)_\Omega - (\mathcal{P}_V \otimes \mathcal{P}_U)_\Omega^T [\mathbf{R}_N(\Omega) + \gamma^2 \mathbf{I}]^{-1} (\mathcal{P}_V \otimes \mathcal{P}_U)_\Omega\}. \end{aligned} \quad (5)$$

Remark: Lemma 2 reveals two key properties of the SMG model. First, *prior* to observing data, part (a) shows that the low-rank matrix \mathbf{X} lies on the linear space \mathcal{T} , and follows a degenerate multivariate Gaussian distribution with mean zero and covariance matrix $\sigma^2(\mathcal{P}_V \otimes \mathcal{P}_U)$ (the Kronecker product of projection matrices for \mathbf{X}). Second, *after* observing the noisy entries \mathbf{Y}_Ω , part (b) shows

that the conditional distribution of \mathbf{X}_{Ω^c} (the unobserved entries in \mathbf{X}) given \mathbf{Y}_{Ω} is still multivariate Gaussian, with closed-form expressions for its mean vector $\mathbf{X}_{\Omega^c}^P$ and covariance matrix $\Sigma_{\Omega^c}^P$ in (4).

2.3 Can we directly use the SMG model for UQ?

Lemma 2 shows that the low-rank matrix \mathbf{X} lies on the space \mathcal{T} and follows a degenerate multivariate Gaussian distribution with mean zero. Moreover, this shows that the posterior distribution of the low-rank matrix \mathbf{X} *after* observing the noisy observations \mathbf{Y}_{Ω} . This can potentially be used to provide the means for computing confidence intervals on each entry in \mathbf{X} , *assuming* the underlying row and column subspaces \mathcal{U} and \mathcal{V} are known. Of course, in practice, such subspace information is never known with certainty. One solution might be to plug in point estimates of \mathcal{U} and \mathcal{V} (estimated from data) within the predictive equations in Lemma 2. We investigate the efficacy of this plug-in approach via a simple numerical example.

Let $m = m_1 = m_2 = 8$ be the matrix dimensions, and let $R = 2$ be its rank. We first simulate two random orthonormal matrices \mathbf{U} and \mathbf{V} of size $m \times R$, via a truncated SVD on an $m \times m$ matrix with i.i.d. $U[0,1]$ entries. With $\mathcal{P}_{\mathcal{U}} = \mathbf{U}\mathbf{U}^T$ and $\mathcal{P}_{\mathcal{V}} = \mathbf{V}\mathbf{V}^T$, the “true” low-rank matrix is then simulated from the SMG model $\mathbf{X} \sim \mathcal{SMG}(\mathcal{P}_{\mathcal{U}}, \mathcal{P}_{\mathcal{V}}, \sigma^2, R)$. Finally, noisy observations are sampled via (1) with noise variance $\eta^2 = 0.5^2$. In total, 36 entries are observed (50% of total entries); such entries are picked uniformly at random. From this, we can obtain point estimates of the subspaces \mathcal{U} and \mathcal{V} , by first estimating \mathbf{X} via nuclear norm minimization (Candès and Plan, 2010), a standard method for matrix completion, and then taking the row and column subspaces for this matrix estimate via an SVD. These subspace estimates are then plugged into the expressions in Lemma 2 for UQ.

Figure 1(a) plots the point estimates and 95% confidence intervals (CIs) for each matrix entry using Lemma 2, with its corresponding true value plotted on the y -axis. Here, the subspaces are estimated via nuclear-norm minimization. We see that the coverage ratio for these plug-in CIs is only 0.5, meaning only half of the confidence intervals cover the true entry value over the matrix. This poor coverage suggests that this confidence interval approach (with plug-in subspaces) can grossly underestimate the underlying uncertainty of our point estimates, which is unsurprising, since uncertainty in subspace estimation is not incorporated into such intervals. Figure 1(b) plots the point estimates and

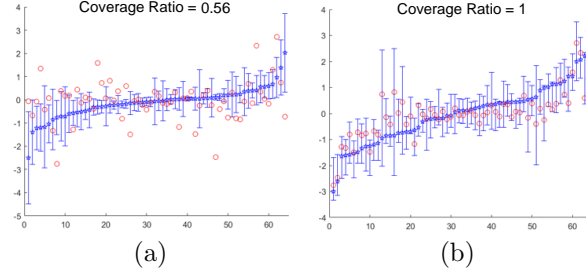


Figure 1: *Plotted are the point estimates (blue points) and 95% CIs (blue intervals) for each matrix entry, ordered by increasing point estimates. Red points mark the true matrix values. Plot (a) makes use of the CIs constructed via Lemma 2 with plug-in subspace estimates; plot (b) uses the posterior predictive intervals from the proposed BayeSMG model.*

95% posterior predictive intervals using the proposed BayeSMG method, which accounts for subspace uncertainty by assigning hierarchical priors on subspaces \mathcal{U} and \mathcal{V} from the SMG model. The resulting coverage ratio is now much higher (at 100%), which is closer to the nominal coverage rate of 95% than the earlier plug-in approach. This shows that the proposed method (presented next) achieves much better uncertainty quantification of \mathbf{X} via a fully-Bayesian model specification on matrix subspaces.

2.4 Bayesian SMG model

We now present the hierarchical specification for the Bayesian SMG model, or the *BayeSMG* model for short. We first describe the matrix von Mises-Fisher distribution on the Stiefel manifold, which will serve as a posterior model for the row and column orthonormal frames \mathbf{U} and \mathbf{V} . Then we present a reparameterization of the SMG model which provides an efficient Gibbs sampler under this prior specification.

The von Mises-Fisher distribution (vMF) is a distributions of subspaces on the Stiefel manifold. A Stiefel manifold, denoted in this paper as $\mathcal{V}_{R,m}$, represents the set of all orthonormal subspaces of rank R in the space of \mathbb{R}^m . Its distribution can be expressed as follows:

$$\left[{}_0F_1\left(\frac{m}{2}; \frac{\mathbf{F}^T \mathbf{F}}{4}\right) \right]^{-1} \text{etr}(\mathbf{F}^T \mathbf{W}), \quad \mathbf{W} \in \mathcal{V}_{R,m}, \quad (6)$$

where ${}_0F_1(\cdot; \cdot)$ is the hypergeometric function. We denote this matrix vMF

distribution as $\mathbf{W} \sim vMF(m, R, \mathbf{F})$ on Stiefel manifold $\mathcal{V}_{R,m}$, where \mathbf{F} is an arbitrary matrix specified (Fisher et al., 1993). In the case of matrix factorization, for instance, $\mathbf{Y} = \mathbf{U}\mathbf{D}\mathbf{V}^T + \mathbf{E}$, where \mathbf{U} and \mathbf{V} are orthonormal matrices, \mathbf{D} is a diagonal matrix with positive entries, and \mathbf{E} consists of independent and identically distributed normal variates. Then, uniform prior distributions of \mathbf{U} and \mathbf{V} in their corresponding Stiefel manifolds will lead to vMF distributions as posteriors, $vMF(\mathbf{Y}\mathbf{V}\mathbf{D}/\sigma^2)$ and $vMF(\mathbf{Y}^T\mathbf{U}\mathbf{D}/\sigma^2)$, respectively.

Efficient sampling algorithms for subspace samples from a matrix vMF distribution are discussed by Hoff (2009) as well. A rejection sampling scheme is proposed to sample the matrix column by column sequentially. For larger values of \mathbf{D} and R , when the rejection sampling will be slow, a Gibbs sampling scheme is proposed instead. Recently, a general approach to Monte Carlo simulation from probability distributions on the Stiefel manifold called *polar expansion* is developed by Jauch et al. (2020). It is observed that the polar expansion with adaptive Hamiltonian Monte Carlo is an order of magnitude more efficient than competing MCMC approaches in some instances.

With the vMF distribution in hand, the following proposition gives a nice reformulation of the SMG model under uniform subspace priors on \mathcal{U} and \mathcal{V} :

Proposition 3 (Singular value decomposition of SMG). *Suppose $\mathbf{X} \sim SMG(\mathcal{P}_{\mathcal{U}}, \mathcal{P}_{\mathcal{V}}, \sigma^2, R)$, with independent uniform priors $\mathcal{P}_{\mathcal{U}} \sim U(\mathcal{G}_{R,m_1-R})$, $\mathcal{P}_{\mathcal{V}} \sim U(\mathcal{G}_{R,m_2-R})$, and fixed σ^2 and R . Let $\mathbf{X} = \mathbf{U}\mathbf{D}\mathbf{V}^T$ be the SVD of \mathbf{X} , with singular values $\text{diag}(\mathbf{D}) = (d_k)_{k=1}^R$ not necessarily in decreasing order. Then:*

1. *The singular vectors \mathbf{U} and \mathbf{V} follow independent uniform priors $U(\mathcal{V}_{R,m_1-R})$ and $U(\mathcal{V}_{R,m_2-R})$, respectively,*
2. *The singular values $\text{diag}(\mathbf{D}) = (d_k)_{k=1}^R$ follow the repulsed normal distribution (Shen, 2001), with density:*

$$\frac{1}{Z_R(2\pi\sigma^2)^{R/2}} \exp \left\{ -\frac{1}{2\sigma^2} \sum_{k=1}^R d_k^2 \right\} \prod_{\substack{k,l=1 \\ k < l}}^R |d_k^2 - d_l^2|, \quad d_k > 0, \quad k = 1, \dots, R. \quad (7)$$

The proof of this proposition is provided in the appendix. Here, the matrix \mathbf{D} is a diagonal matrix with singular values following the repulsed normal distribution. This is transformed from the latent matrix \mathbf{Z} . This first proposition connects the uniform prior in $\mathcal{P}_{\mathcal{U}}$ and $\mathcal{P}_{\mathcal{V}}$ to the uniform prior in subspace matrices \mathbf{U}

Table 1: Model specification for BayeSMG.

<i>Model</i>	<i>Distribution</i>
Observations	$[\mathbf{Y}_\Omega \mathbf{X}, \eta^2]: Y_{i,j} \stackrel{i.i.d.}{\sim} \mathcal{N}(X_{i,j}, \eta^2)$
Low-rank matrix	$[\mathbf{X} \mathcal{P}_U, \mathcal{P}_V, \sigma^2]: \mathbf{X} \sim \mathcal{SMG}(\mathcal{P}_U, \mathcal{P}_V, \sigma^2, R)$
Priors	$[\mathcal{P}_U, \mathcal{P}_V, \sigma^2, \eta^2] = [\mathcal{P}_U] [\mathcal{P}_V] [\eta^2] [\sigma^2]$
Matrix subspaces	$[\mathcal{P}_U] \sim U(\mathcal{G}_{R, m_1 - R}), \quad [\mathcal{P}_V] \sim U(\mathcal{G}_{R, m_2 - R})$
Matrix variance	$[\sigma^2] \sim IG(\alpha_{\sigma^2}, \beta_{\sigma^2})$
Noise variance	$[\eta^2] \sim IG(\alpha_{\eta^2}, \beta_{\eta^2})$

and \mathbf{V} . This motivates us for the choice of the uniform and the repulsed normal distribution priors in the model to be compatible with the SMG distribution, which helps with the derivation of the posterior distribution.

Here, if we do not have additional information about the subspace, we can use the non-informative prior in SMG. In other words, we can assume the subspace distribution \mathbf{U} and \mathbf{V} to be uniformly distributed on the manifold:

$$[\mathcal{P}_U] \sim U(\mathcal{G}_{R, m_1 - R}), \quad [\mathcal{P}_V] \sim U(\mathcal{G}_{R, m_2 - R}). \quad (8)$$

It is also possible to use the vMF distribution as prior distribution to incorporate additional information on the subspaces. For the variance parameters σ^2 and η^2 , we assign the non-informative priors:

$$[\eta^2] \sim IG(\alpha_{\eta^2}, \beta_{\eta^2}), \quad [\sigma^2] \sim IG(\alpha_{\sigma^2}, \beta_{\sigma^2}), \quad (9)$$

where $IG(\alpha, \beta)$ is the Inverse-Gamma distribution with shape and rate parameters α and β . These Inverse-Gamma priors provide the so-called conjugate priors Gelman et al. (2014) for the proposed model, which allow for an efficient, closed-form sampling scheme for UQ (see Section 3). The full model is summarized in Table 1.

In practice, we can use several ways for prior elicitation for the subspaces. One conventional way is to do moment matching, where we set the mean and variance for the subspace priors the same to empirical distribution (Wang and Zhou, 2009). For non-symmetric distributions, we can utilize quantile-based methods instead (Dey et al., 2007).

3 Subspace Gibbs sampler for posterior sampling

Using the reparametrization model from Proposition 3, we now present a subspace Gibbs sampler for posterior sampling on the BayeSMG model, specifically on the parameters $\Theta = \{\mathbf{U}, \mathbf{D}, \mathbf{V}, \sigma^2\}$ given partial and noisy observations \mathbf{Y}_Ω . We will first introduce the sampler under *complete* observation of the noisy matrix \mathbf{Y} , then describe a data imputation procedure for posterior sampling under *partial* observations \mathbf{Y}_Ω .

Assume for now that complete observations \mathbf{Y} are obtained. Then the full conditional distributions of \mathbf{U} , \mathbf{D} , \mathbf{V} and σ^2 can be derived as follows:

$$\begin{aligned} [\mathbf{U}|\mathbf{D}, \mathbf{V}, \mathbf{Y}, \sigma^2, \eta^2] &\sim vMF(m_1, R, \mathbf{YVD}/\eta^2), \\ [\mathbf{V}|\mathbf{D}, \mathbf{U}, \mathbf{Y}, \sigma^2, \eta^2] &\sim vMF(m_2, R, \mathbf{Y}^T \mathbf{UD}/\eta^2), \\ [\mathbf{D}|\mathbf{U}, \mathbf{V}, \mathbf{Y}, \sigma^2, \eta^2] &\sim \mathcal{RN}(\sigma^2 \text{diag}(\mathbf{U}^T \mathbf{YV})/(\eta^2 + \sigma^2), \eta^2 \sigma^2/(\eta^2 + \sigma^2)), \\ [\sigma^2|\mathbf{U}, \mathbf{D}, \mathbf{V}, \mathbf{Y}, \eta^2] &\sim IG(\alpha_{\sigma^2} + R/2, \beta_{\sigma^2} + \text{tr}(\mathbf{D}^2)/2), \\ [\eta^2|\mathbf{U}, \mathbf{D}, \mathbf{V}, \mathbf{Y}, \sigma^2] &\sim IG(\alpha_{\eta^2} + m_1 m_2/2, \beta_{\eta^2} + \|\mathbf{Y} - \mathbf{UDV}^T\|_F^2/2). \end{aligned}$$

Based on the posterior distribution, one can then sample for all parameters $[\Theta|\mathbf{Y}]$ given *complete* observations \mathbf{Y} via Gibbs sampling, by performing the above full conditional updates cyclically. The detailed proof is in Appendix A.4. As stated in Proposition 3, The distributions for singular values in the model is the repulsed normal distribution, noted as $\mathcal{RN}(\boldsymbol{\mu}, \delta^2)$:

$$\frac{1}{Z_R(2\pi\delta^2)^{R/2}} \exp \left\{ -\frac{1}{2\delta^2} \sum_{k=1}^R (d_k - \mu_k)^2 \right\} \prod_{k,l=1; k < l}^R |d_k^2 - d_l^2|, \quad (10)$$

where $d_k > 0, k = 1, \dots, R$. It can be efficiently sampled via a Metropolis-Hastings independence sampler, with the proposed distribution being a non-central, multivariate t -distribution with mean vector $\boldsymbol{\mu}$ and scale parameter δ .

We can then make use of a simple modification of the above steps (which generate samples from the posterior distribution $[\Theta|\mathbf{Y}]$ given the *full* observation matrix \mathbf{Y}), to generate samples from the desired posterior distribution $[\Theta|\mathbf{Y}_\Omega]$ given the *partial* observations \mathbf{Y}_Ω . The idea is to first sample from the joint distribution $[\Theta, \mathbf{Y}_{\Omega^c}|\mathbf{Y}_\Omega]$ of both parameters Θ and unobserved noisy entries \mathbf{Y}_{Ω^c} , then take only the marginal samples of parameters Θ . The joint distribution $[\Theta, \mathbf{Y}_{\Omega^c}|\mathbf{Y}_\Omega]$ can be sampled via the following Gibbs steps.

Algorithm 1 BayeSMG($\mathbf{Y}_\Omega, R, \alpha_{\sigma^2}, \beta_{\sigma^2}, \alpha_{\eta^2}, \beta_{\eta^2}$): Gibbs sampler for BayeSMG

Initialization: Complete $\mathbf{X}_{[0]}$ from \mathbf{Y}_Ω via nuclear-norm minimization.

Initialize $[\mathbf{U}_{[0]}, \mathbf{D}_{[0]}, \mathbf{V}_{[0]}] \leftarrow \text{svd}(\mathbf{X}_{[0]})$ and $\sigma_{[0]}^2$.

Gibbs sampler:

T - total samples

for $t = 1, \dots, T$ **do**

$\mathbf{X}_{[t]} \leftarrow \mathbf{U}_{[t-1]} \mathbf{D}_{[t-1]} \mathbf{V}_{[t-1]}^T$
 With \mathbf{Y}_Ω fixed, impute missing entries \mathbf{Y}_{Ω^c} by sample
 $Y_{i,j} \sim X_{[t],i,j} + \mathcal{N}(0, \eta^2), \quad (i, j) \in \Omega^c$.
 Sample $\mathbf{U}_{[t]} \sim vMF(m_1, R, \mathbf{Y} \mathbf{V}_{[t-1]} \mathbf{D}_{[t-1]} / \eta_{[t-1]}^2)$.
 Sample $\mathbf{V}_{[t]} \sim vMF(m_2, R, \mathbf{Y}^T \mathbf{U}_{[t]} \mathbf{D}_{[t-1]} / \eta_{[t-1]}^2)$.
 Sample $\mathbf{D}_{[t]} \sim \mathcal{RN} \left(\frac{\sigma_{[t-1]}^2 \text{diag}(\mathbf{U}_{[t]}^T \mathbf{Y} \mathbf{V}_{[t]})}{\eta_{[t-1]}^2 + \sigma_{[t-1]}^2}, \frac{\eta_{[t-1]}^2 \sigma_{[t-1]}^2}{\eta_{[t-1]}^2 + \sigma_{[t-1]}^2} \right)$.
 Sample $\sigma_{[t]}^2 \sim IG(\alpha_{\sigma^2} + R/2, \beta_{\sigma^2} + \text{tr}(\mathbf{D}_{[t]}^2)/2)$.
 Sample $\eta_{[t]}^2 \sim IG(\alpha_{\eta^2} + m_1 m_2 / 2, \beta_{\eta^2} + \|\mathbf{Y} - \mathbf{U}_{[t]} \mathbf{D}_{[t]} \mathbf{V}_{[t]}^T\|_F^2 / 2)$.

Output: Return posterior samples $\{(\mathbf{X}_{[t]}, \mathbf{U}_{[t]}, \mathbf{D}_{[t]}, \mathbf{V}_{[t]}, \sigma_{[t]}^2, \eta_{[t]}^2)\}_{t=1}^T$.

- (i) First sample from the posterior distribution for the parameters given all observed and unobserved entries $[\Theta | \mathbf{Y}_{\Omega^c}, \mathbf{Y}_\Omega] = [\Theta | \mathbf{Y}]$. This can be done by following the conditional posteriors derived in (10).
- (ii) Subsequently sample from $[\mathbf{Y}_{\Omega^c} | \mathbf{Y}_\Omega, \Theta]$. Since \mathbf{Y}_{Ω^c} is independent of \mathbf{Y}_Ω given $\mathbf{X} = \mathbf{U} \mathbf{D} \mathbf{V}^T$, this is equivalent to sampling $[\mathbf{Y}_{\Omega^c} | \mathbf{X}]$, which amounts to simulating the observation noise in \mathbf{Y}_{Ω^c} given ground truth $\mathbf{X} = \mathbf{U} \mathbf{D} \mathbf{V}^T$.

The second step can be viewed as a data imputation step, which is connected to missing data. In the literature, the missing data is usually assumed to be “missing-at-random” (typically to ensure subsequent theoretical performance guarantee); here, we assume that the locations of the missing entries Ω are known.

The full BayeSMG sampling algorithm is detailed in Algorithm 1, including the choice of prior distributions and the full conditional posterior distributions derived in the previous section.

Quantifying uncertainty from the MCMC samples is the key to UQ by the BayeSMG model. With the parameters sampled in each iteration, we may obtain a sample of $\mathbf{X} = \mathbf{U} \mathbf{D} \mathbf{V}^T$ for each iteration, which contains all the entries, observed or unobserved. Taking the mean value of all such samples will produce a mean estimate of the matrix. When considering the matrix entry by entry, the highest posterior density range is used to provide the precision of the estimates, fulfilling the uncertainty quantification objective. Additionally, the run time

of the algorithm is relatively short, given the complexity of the algorithm. For instance, a typical Gibbs sampler execution on a 256×256 matrix with half of its entries missing is around 60 seconds, indicating the algorithm's efficiency is adequate.

4 Theoretical insights

4.1 Connection to regularized estimators

The following lemma reveals an inherent connection between the BayeSMG model and existing completion methods:

Lemma 4 (MAP estimator). *Assume the model in Table 1, with $\pi_r \propto 1$, and η^2 and σ^2 fixed. Conditional on \mathbf{Y}_Ω , the maximum-a-posteriori (MAP) estimator for \mathbf{X} becomes*

$$\operatorname{argmin}_{\mathbf{X} \in \mathbb{R}^{m_1 \times m_2}} \left(\frac{\|\mathbf{Y}_\Omega - \mathbf{X}_\Omega\|_2^2}{\eta^2} + \log(2\pi\sigma^2) \operatorname{rank}^2(\mathbf{X}) + \frac{\|\mathbf{X}\|_F^2}{\sigma^2} \right), \quad (11)$$

where $\|\mathbf{X}\|_F = \sqrt{\sum_{i,j} X_{i,j}^2}$ is the Frobenius norm of \mathbf{X} .

The MAP estimator $\tilde{\mathbf{X}}$ in (11) reveals an illuminating connection between our model and existing (deterministic) matrix completion methods (see Davenport and Romberg (2016) and references therein). Consider the following approximation to the MAP formulation (11). Treating $\log(2\pi\sigma^2) \operatorname{rank}^2(\mathbf{X})$ as a Lagrange multiplier, and replace the rank function $\operatorname{rank}(\mathbf{X})$ by its nuclear norm $\|\mathbf{X}\|_*$ (its tightest convex relaxation (Keshavan et al., 2010)), the optimization in (11) becomes:

$$\operatorname{argmin}_{\mathbf{X} \in \mathbb{R}^{m_1 \times m_2}} \|\mathbf{Y}_\Omega - \mathbf{X}_\Omega\|_2^2 + \lambda \{ \alpha \|\mathbf{X}\|_* + (1 - \alpha) \|\mathbf{X}\|_F^2 \}, \quad (12)$$

for some choice of $\lambda > 0$ and $\alpha \in (0, 1)$. Using (12) to approximate (11), we can then view the MAP estimator as an analogue of the *elastic net* estimator (Zou and Hastie, 2005) from linear regression for noisy matrix completion.

To see the connection between the MAP estimator $\tilde{\mathbf{X}}$ and existing matrix completion methods, set $\alpha = 1$ in (12). The problem then reduces to:

$$\hat{\mathbf{X}} = \operatorname{argmin}_{\mathbf{X} \in \mathbb{R}^{m_1 \times m_2}} \left(\sum_{(i,j) \in \Omega} (Y_{i,j} - X_{i,j})^2 + \lambda \|\mathbf{X}\|_* \right), \quad (13)$$

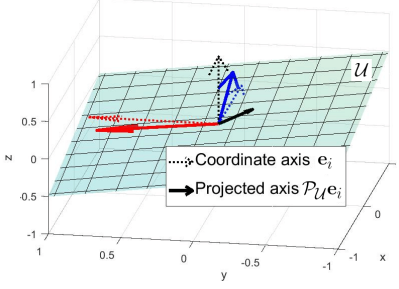


Figure 2: A visualization of near-maximal coherence (red basis vector) and minimal coherence (black basis vector) for subspace \mathcal{U} .

which is precisely the nuclear-norm formulation widely used for matrix completion (Candès and Recht, 2009; Candès and Tao, 2010; Recht, 2011).

4.2 Uncertainty and coherence

Consider the following definition of subspace coherence from Candès and Recht (2009) (ignoring scaling factors):

Definition 5 (Coherence). (*Definition 1.2, (Candès and Recht, 2009)*) Let $\mathcal{U} \in \mathcal{G}_{R,m-R}$ be an R -plane in \mathbb{R}^m , and let $\mathcal{P}_{\mathcal{U}}$ be the orthogonal projection onto \mathcal{U} . The coherence of subspace \mathcal{U} with respect to the i -th basis vector, \mathbf{e}_i , is defined as $\mu_i(\mathcal{U}) := \|\mathcal{P}_{\mathcal{U}}\mathbf{e}_i\|_2^2$, and the coherence of \mathcal{U} is defined as $\mu(\mathcal{U}) = \max_{i=1,\dots,m} \mu_i(\mathcal{U})$.

In words, coherence measures how *correlated* a subspace \mathcal{U} is with the basis vectors $\{\mathbf{e}_i\}_{i=1}^m$. A large $\mu_i(\mathcal{U})$ suggests that \mathcal{U} is highly correlated with the i -th basis vector \mathbf{e}_i , in that the projection of \mathbf{e}_i onto \mathcal{U} preserves much of its original length; a small value of $\mu_i(\mathcal{U})$ suggests that \mathcal{U} is nearly orthogonal with \mathbf{e}_i , so a projection of \mathbf{e}_i onto \mathcal{U} loses most of its length. Figure 2 visualizes these two cases using the projection of three basis vectors on a two-dimensional subspace \mathcal{U} . Note that the projection of the red vector onto \mathcal{U} retains nearly unit length, so \mathcal{U} has near-maximal coherence for this basis. The projection of the black vector onto \mathcal{U} results in a considerable length reduction, so \mathcal{U} has near-minimal coherence for this basis. Here, the overall coherence of \mathcal{U} , $\mu(\mathcal{U})$, is largely due to the high coherence of the red basis vector.

In matrix completion literature, coherence is widely used to quantify the *recoverability* of a low-rank matrix \mathbf{X} . Here, the same notion of coherence arises

in a different context within the proposed model’s uncertainty quantification. Lemma 2 provides the basis for this connection. Consider first the case where no matrix entries have been observed. From Lemma 2(a), $\text{vec}(\mathbf{X})$ follows the degenerate Gaussian distribution $\mathcal{N}\{\mathbf{0}, \sigma^2(\mathcal{P}_{\mathcal{V}} \otimes \mathcal{P}_{\mathcal{U}})\}$. The variance of the (i, j) -th entry in \mathbf{X} can then be shown to be:

$$\text{Var}(X_{i,j}) = \sigma^2(\mathbf{e}_i^T \mathcal{P}_{\mathcal{U}} \mathbf{e}_i)(\mathbf{e}_j^T \mathcal{P}_{\mathcal{V}} \mathbf{e}_j) = \sigma^2 \mu_i(\mathcal{U}) \mu_j(\mathcal{V}). \quad (14)$$

Hence, before observing data, the model uncertainty for entry $X_{i,j}$ is proportional to the product of coherences for the row and column spaces \mathcal{U} and \mathcal{V} , with respect to the i -th and the j -th basis vectors. Put another way, *the proposed model assigns greater variation to matrix entries with high subspace coherence in either its row or column index*. This is quite appealing in view of the original role of coherence in matrix completion, where larger row (or column) coherences imply greater “spikiness” for entries; our framework accounts for this by assigning greater *model uncertainty* to such entries.

Consider next the case where noisy entries \mathbf{Y}_{Ω} have been observed. Consider a slightly generalized notion of coherence:

Definition 6 (Cross-coherence). *The cross-coherence of subspace \mathcal{U} with respect to the basis vectors \mathbf{e}_i and $\mathbf{e}_{i'}$ is defined as $\nu_{i,i'}(\mathcal{U}) = \mathbf{e}_{i'}^T \mathcal{P}_{\mathcal{U}} \mathbf{e}_i$.*

The cross-coherence $\nu_{i,i'}(\mathcal{U})$ quantifies how correlated the basis vectors \mathbf{e}_i and $\mathbf{e}_{i'}$ are, *after* a projection onto \mathcal{U} . For example, in Figure 2, the pair of red / blue projected basis vectors have negative cross-coherence for \mathcal{U} , whereas the pair of blue / black projected vectors have positive cross-coherence. When $i = i'$, this cross-coherence reduces to the original coherence.

Define now the cross-coherence vector $\boldsymbol{\nu}_i(\mathcal{U}) = [\nu_{i,i_n}(\mathcal{U})]_{n=1}^N \in \mathbb{R}^N$, where again $\Omega = \{(i_n, j_n)\}_{n=1}^N$. From equation (4) in Lemma 2, the conditional variance of entry $X_{i,j}$ for an unobserved index $(i, j) \in \Omega^c$ becomes:

$$\text{Var}(X_{i,j} | \mathbf{Y}_{\Omega}) = \sigma^2 \mu_i(\mathcal{U}) \mu_j(\mathcal{V}) - \sigma^2 \boldsymbol{\nu}_{i,j}^T [\mathbf{R}_N(\Omega) + \gamma^2 \mathbf{I}]^{-1} \boldsymbol{\nu}_{i,j}, \quad (15)$$

where $\boldsymbol{\nu}_{i,j} := \boldsymbol{\nu}_i(\mathcal{U}) \circ \boldsymbol{\nu}_j(\mathcal{V})$, and \circ denotes the entry-wise (Hadamard) product. The expression in (15) also enjoys a nice interpretation. From a UQ perspective, the first term in (15), $\mu_i(\mathcal{U}) \mu_j(\mathcal{V})$, is simply the unconditional uncertainty for entry $X_{i,j}$, *prior* to observing data. The second term, $\boldsymbol{\nu}_{i,j}^T [\mathbf{R}_N(\Omega) + \gamma^2 \mathbf{I}]^{-1} \boldsymbol{\nu}_{i,j}$, can be viewed as the *reduction* in uncertainty, *after* observing the noisy entries \mathbf{Y}_{Ω} . This uncertainty reduction is made possible by the correlation structure

imposed on \mathbf{X} , via the SMG model; (15) also yields valuable insight in terms of subspace correlation. The first term $\mu_i(\mathcal{U})\mu_j(\mathcal{V})$ can be seen as the joint correlation between (i) row space \mathcal{U} to row index i , and (ii) column space \mathcal{V} to column index j , *prior* to any observations. The second term can be viewed as the portion of this correlation *explained* by observed indices Ω .

4.3 Error monotonicity

Using this link between coherence and uncertainty, we present two novel insights on expected error decay. The following theorem forms the basis for these insights:

Theorem 7 (Variance reduction). *Suppose \mathcal{U} and \mathcal{V} are fixed. Let \mathbf{Y}_Ω contain the entries at $\Omega \subseteq [m_1] \times [m_2]$, and let $\mathbf{Y}_{\Omega \cup (i,j)}$ contain an additional observation at $(i,j) \in \Omega^c$. For any index $(k,l) \in [m_1] \times [m_2]$, the conditional variance of $X_{k,l}$ can be decomposed as*

$$\text{Var}(X_{k,l}|\mathbf{Y}_{\Omega \cup (i,j)}) = \text{Var}(X_{k,l}|\mathbf{Y}_\Omega) - \frac{\text{Cov}^2(X_{k,l}, X_{i,j}|\mathbf{Y}_\Omega)}{\text{Var}(X_{i,j}|\mathbf{Y}_\Omega) + \eta^2}, \quad (16)$$

where $\text{Cov}(X_{i,j}, X_{k,l}|\mathbf{Y}_\Omega) = \sigma^2\{\nu_{i,k}(\mathcal{U})\nu_{j,l}(\mathcal{V}) - \boldsymbol{\nu}_{i,j}^T [\mathbf{R}_N(\Omega) + \gamma^2\mathbf{I}]^{-1} \boldsymbol{\nu}_{k,l}\}$.

Remark: Theorem 7 shows that given observed indices Ω , the reduction in uncertainty (as measured by variance) for an unobserved entry $X_{k,l}$, after observing an additional entry at index (i,j) . The last term in (16) quantifies this reduction, and can be interpreted as follows. For an unobserved index $(k,l) \notin \Omega \cup (i,j)$, the amount of uncertainty reduction is related to the “*signal-to-noise*” ratio, where the signal is the conditional squared-covariance between the “unobserved” entry $X_{k,l}$ and the “to-be-observed” entry $X_{i,j}$, and the noise is the conditional variance of the “to-be-observed” entry.

The insight of *error monotonicity* follows immediately:

Corollary 1 (Error monotonicity). *For an arbitrary sequential sampling scheme, suppose \mathcal{U} and \mathcal{V} are fixed. Let $[(i_n, j_n)]_{n=1}^{m_1 m_2} \subseteq [m_1] \times [m_2]$ be an arbitrary sampling scheme, where $(i_n, j_n) \neq (i_{n'}, j_{n'})$ for $n \neq n'$. Let $X_{k,l}^P$ be the (k,l) -th entry of the conditional mean in (4). Define*

$$\epsilon_N^2(k,l) := \mathbb{E} \left\{ (X_{k,l} - X_{k,l}^P)^2 \mid \mathbf{Y}_{\Omega_{1:N}} \right\}, \quad (k,l) \in [m_1] \times [m_2]$$

as the expected squared-error for $X_{k,l}$ after observing $\mathbf{Y}_{\Omega_{1:N}}$. Then $\epsilon_{N+1}^2(k,l) < \epsilon_N^2(k,l)$ for any $N = 1, 2, \dots$.

Remark: This corollary shows that for any sequential sampling scheme and any index (k, l) , the expected squared-error in estimating $X_{k,l}$ with the conditional mean $X_{k,l}^P$ is always monotonically decreasing as more samples are collected. This is intuitive since one expects to gain greater accuracy and precision on the unknown matrix \mathbf{X} as more entries are observed. The fact that the proposed model quantifies this monotonicity property provides a reassuring check on our UQ approach.

5 Numerical experiments

We now investigate the performance of the proposed BayeSMG method in numerical simulations and compare it to the aforementioned BPF method (Salakhutdinov and Mnih, 2008), a popular Bayesian matrix completion method in the literature.

5.1 Synthetic data

For the first numerical study, we assume the true matrix \mathbf{X} is generated from the SMG distribution, i.e., as $\mathbf{X} \sim \mathcal{SMG}(\mathcal{P}_{\mathcal{U}}, \mathcal{P}_{\mathcal{V}}, \sigma^2 = 1, R)$, with uniformly sampled subspaces \mathcal{U} and \mathcal{V} . The matrix \mathbf{X} entries are assumed to be missing-at-random and the observed entries are contaminated by noise with a variance $\eta^2 = 0.05^2$, which we presume to be known. The prior specifications are as follows. For BayeSMG, we assign a weakly-informative prior $\sigma^2 \sim IG(0.01, 0.01)$ on the variance parameter σ^2 ; for BPF, we assign the recommended weak Inverse-Wishart priors on covariance matrices $\Sigma_m \sim IW(R = 2, \mathbf{I})$, $\Sigma_n \sim IW(R = 2, \mathbf{I})$. We then ran 10,000 MCMC iterations for both methods, with the first 2,000 samples taken as burn-in. Standard MCMC convergence checks were performed via trace plot inspection (see Figure 3 (b)) and the Gelman-Rubin statistic (Gelman and Rubin, 1992).

We employ two metrics to compare the posterior contraction (and thereby the uncertainty quantification) performance of these two methods. The first is the Mean Frobenius Error (MFE), defined as

$$\text{MFE} = (1/T) \sum_{t=1}^T \|\mathbf{X} - \mathbf{X}_{[t]}\|_F.$$

The MFE calculates the Frobenius norm of the difference between the posterior

predictive samples $\{\mathbf{X}_{[t]}\}_{t=1}^T$ and the true matrix \mathbf{X} . A smaller MFE suggests better recovery and faster posterior contraction for the desired matrix \mathbf{X} . The second metric is the Mean Spectral Distance (MSD), defined as

$$\text{MSD} = (1/T) \sum_{t=1}^T d_S(\mathcal{U}, \mathcal{U}_{[t]}), \quad d_S(\mathcal{U}, \mathcal{U}') := \sqrt{1 - \|\mathbf{U}^T \mathbf{U}'\|_2^2}.$$

The MSD calculates the spectral distance (Calderbank et al., 2015) between the posterior samples $\{\mathcal{U}_{[t]}\}_{t=1}^T$ for the row subspaces (equivalently, $\{\mathcal{V}_{[t]}\}_{t=1}^T$ for the column subspaces) and the true row subspace \mathcal{U} (equivalently, the true column subspace \mathcal{V}). A smaller MSD suggests better recovery and posterior contraction for matrix subspaces.

The first two plots in Figure 3(a) visualize the true matrix \mathbf{X} and the observed \mathbf{Y}_Ω , with 20% of the entries observed uniformly-at-random. The next two plots visualize the posterior mean estimates for \mathbf{X} using BayeSMG and BPMF. We see that the BayeSMG method provides a visually better recovery of the matrix \mathbf{X} , with a lower posterior MFE than the BPMF method. The first two plots in Figure 3(b) visualize the true and estimated row spaces using BayeSMG and BPMF. We again see that BayeSMG gives a visually better recovery of the row space of \mathbf{X} (the same holds for its column space), with a lower posterior MSD than BPMF. The next two plots show the trace plots for the first row coherence μ_1 and the first matrix entry $X_{1,1}$, which is unobserved. We see that the posterior samples for BayeSMG concentrate tightly around the true coherence and matrix values, whereas the posterior samples for BPMF fluctuate much more around the truth. The above observations suggest that, when the true matrix is generated from the assumed prior model, BayeSMG yields much faster posterior contraction than BPMF, leading to more accurate and precise estimates of \mathbf{X} and its subspaces. We show next, in the following image recovery experiments and seismic sensor application, that the proposed method provides similar improvements over BPMF by learning and integrating subspace information for recovery.

5.2 Image inpainting

Image inpainting is a fundamental problem (Bertalmio et al., 2000; Cai et al., 2010), which aims to recover and reconstruct images with missing pixels and noise corruption. It is of great importance in image processing since image data are

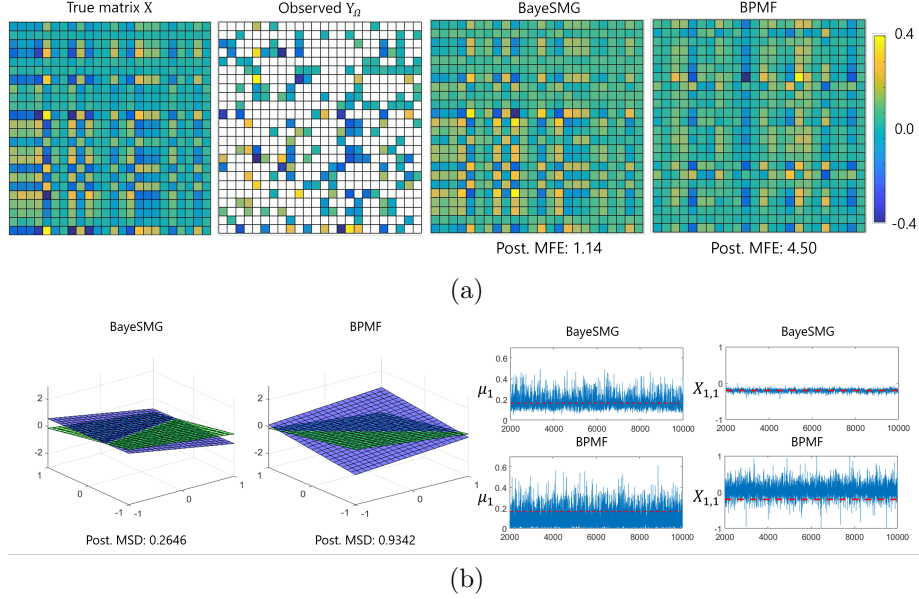


Figure 3: Recovery and UQ performance for a simulated 25×25 matrix. In (a), the four plots show (from left to right) the true matrix \mathbf{X} , observations \mathbf{Y}_Ω , and the posterior mean estimates from BayeSMG and BPMF. In (b), the left plots visualize the true row space (green) and estimated row space (blue) from BayeSMG and BPMF for the first two dimensions, with posterior MSD calculated. On the right are the trace plots for row coherence μ_1 and an unobserved entry $X_{1,1}$, for BayeSMG and BPMF, with true values dotted in red.

often susceptible to unreliable data transmission and scratches. Take, for example, the problem of solar imaging (Xie et al., 2012). When a satellite transmits an image of the sun back to the earth, many pixels will inevitably be lost or corrupted due to the instabilities in the transmission process. Furthermore, missing pixels would need to be filled in when the image is being scaled up. Here, both the recovery of the image and the quantification of its uncertainty are important; since the uncertainty quantification can provide additional information about the quality of recovered image features in different regions. There has been some work on applying (deterministic) matrix completion methods for image in-painting, see, e.g., Xue et al. (2017), but little has been done on uncertainty quantification. Our method addresses the latter goal.

We consider the aforementioned solar imaging problem, where the matrix \mathbf{X} is a 256×256 image solar flare. The pixel intensity value is encoded from 0 to 255 and represented using pseudo-color in the images. We then normalize these

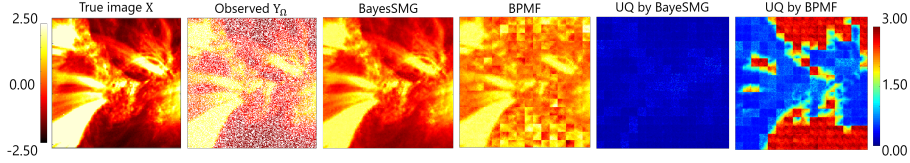


Figure 4: Performance comparison between *BayeSMG* and *BPFM* on a 256×256 solar flare image. The plots (from left to right) show the original image, the partially observed image with noise, the recovered images using *BayeSMG* and *BPFM*, and the widths of the entry-wise 95% HPD intervals from *BayeSMG* and *BPFM*.

pixel intensities to have zero mean and variance $\sigma^2 = 1$. Half of the pixels in this image are observed uniformly at random, then corrupted by Gaussian noise $\eta^2 = 0.05^2$. We note that, for this problem, the recovery and UQ of the row and column subspaces are of interest as well. This is because image features are often represented in the row and column spaces. Here, these subspaces may quantify domain-specific, interpretable phenomena, such as different classes of solar flares, certain shapes, and sunspots. Furthermore, human eyes are typically not as sensitive to high-frequency image features; therefore, a few SVD components can often capture the vital features of an image, making its rank low. We take 1,000 iterations in MCMC to estimate the parameters, with a 200 burn-in period. After the iterations, we check a few entry estimates and ensure the MCMC has converged.

Figure 4 shows the true solar image, its partial observations, and the recovered image using *BayeSMG* and *BPFM* (via its posterior predictive mean) as well as its corresponding uncertainties (via its 95% highest posterior density (HPD) interval width). We see that the *BayeSMG* method provides a much better recovery of the image, with a much lower MFE of 31.0 compared to the *BPFM* method (350.8). Visually, we see that the *BayeSMG* recovery captures the key features of the image, e.g., different types of solar flares. The *BPFM* recovery, on the other hand, loses much of the smaller-scale features and contains significant blocking defects. One plausible explanation is that, when low-rank subspace structure is present in \mathbf{X} (as is the case here), the proposed method can better learn and integrate this structure for improved recovery. Furthermore, an inspection of the HPD plots shows that the *BayeSMG* is quite certain of the recovered image, with narrow posterior intervals across the whole matrix. In contrast, the *BPFM* is much more uncertain of its recovery: its entry-wise posterior intervals are considerably wider, particularly for pixels with low intensities. Computation-

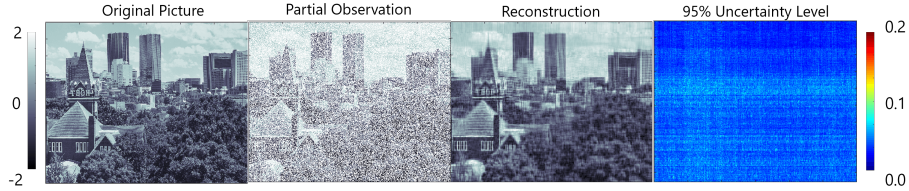


Figure 5: Performance of BayeSMG on recovering a large 1911×3000 image of the Georgia Tech campus. The four plots show (from left to right) the original image, the partial observations, the recovered image using BayeSMG, and the widths of the entry-wise 95% HPD intervals from BayeSMG.

wise, the posterior sampling for BayeSMG can be performed within one minute on a standard laptop computer (Intel i7 processor and RAM space of 16GB), which is quite fast, considering the relatively large size of the image.

To demonstrate the scalability of BayeSMG, we consider next a much higher-dimensional image of the Georgia Tech campus. This image is converted to a gray-scale matrix of size 1911×3000 . As before, half of the pixels are observed uniformly at random, then corrupted by a Gaussian noise $\eta^2 = 0.05^2$. We run the MCMC for 100 iterations after the burn-in period.

Figure 5 shows the true image, its partial observations, and the recovered image from BayeSMG as well as its corresponding uncertainty. The MFE of this recovery is 1005.1, which is again noticeably smaller than that for the BPMF recovery (3004.8). We see that the recovered BayeSMG image captures the original image’s key features, which again shows that the proposed method can learn and integrate the subspace structure for recovery. As before, the BayeSMG is quite certain of this recovery, with narrow posterior HPD intervals over all pixels. Despite this being a much larger image, BayeSMG can again be performed on the same standard laptop, albeit with a longer time of 24 minutes. This shows that, in addition to improved recovery performance and reduced uncertainty, the proposed method is quite scalable for high-dimensional matrices as well.

6 Application to seismic sensor networks

Seismic imaging has long been used to find oil and natural gas beneath the surface of the earth. Ambient Noise Seismic Imaging (Bensen et al., 2007) is a relatively new technique for seismic imaging with great potential, which uses “ambient noises” instead of actively collected signals and is non-invasive to the environment (compared to the traditional active imaging techniques). ANSI

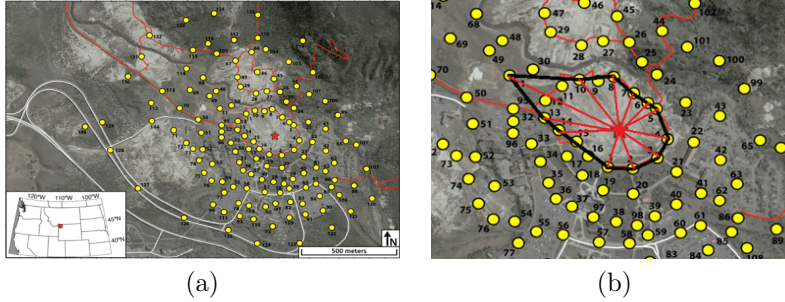


Figure 6: The location of all 132 sensors near the geyser in Yellowstone National Park. The yellow circles indicate the sensors and the red pentagram indicates the location of the geyser. (a) shows the distribution of all 132 sensors over the region close to the geyser as in Xu et al. (2019); (b) shows the locations of the 12 most significant sensors and their relative direction from each other.

has proved to be very useful for imaging shallow earth structures; it is based on pairwise cross-correlation function between signals recorded by seismic sensors followed by time-frequency analysis. In a study (Xu et al., 2019) on the Old Faithful geyser at Yellowstone National Park, 132 sensors are deployed in its vicinity to collect the ambient noise signals to investigate the geological structure. Figure 6(a) shows the locations of these sensors.

However, one limitation of ANSI is that many pairwise cross-correlations do not have any useful “signal” (the peak in the cross-correlation is not observed), since it is based on weak ambient noises. This missing data then results in missing entries in the cross-correlation matrix. We first locate the pairwise correlations that have a satisfactory signal-to-noise ratio as “missing” data. To determine whether the cross-correlation is corrupted, we look at the variance outside of the main lobe relative to the magnitude of the peak \hat{g} : such that if $\hat{g}/\sigma < 20$. We then record its time shift as an entry into the matrix for the pairs with strong correlation. We call this cross-correlation matrix with missing entries as the noisy observed matrix \mathbf{Y}_Ω , plotted in Figure 7. The matrix entries are observed with noise due to the background vibration in the ground. It is estimated from the signals that $\eta = 0.05$.

To proceed with ANSI analysis, one would need to estimate the missing entries in the cross-correlation matrix \mathbf{X} . It is shown in (Bensen et al., 2007) that such a matrix is indeed low-rank. Thus we can then apply the proposed BayeSMG method to recover this matrix for seismic imaging. UQ is of critical importance for the estimation of geologic structure and source of activities. By incorporating uncertainty, we will make more sense of the wave tomography generated from the

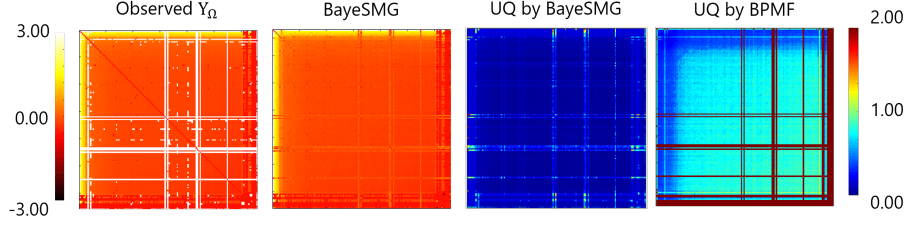


Figure 7: Performance comparison between BayeSMG and BPFM on ambient noise cross-correlation data matrix. The first plot (from the left) shows the observed entries in the cross-correlation matrix, with missing entries colored white. The second plot shows the completed matrix using BayeSMG. The third and fourth plots visualize the widths of the entry-wise 95% HPD intervals from BayeSMG and BPFM.

time delay estimates, knowing the parts where the estimates are accurate and where they are not. This will, in turn, guide the accuracy of analysis downstream, improving the understanding of the quality of reconstruction.

Figure 7 visualizes the recovery performance from BayeSMG and UQ using BayesSMG and BPFM. It is reflected in Figure 7 that BayeSMG has a clear edge over BPFM both in the widths of uncertainty. This can be due to the modeling of subspace in the former approach, where obvious features occur (the bright stripes in the left and top edge of the matrix plot). These subspace reflect several sensors that clearly correlate with each other, indicating potential connections between them due to their relative locations. We utilize the completed matrix to find such sensors most significantly correlated with each other, shown in Figure 6(b). They are expected to be of more importance in further seismic studies. This is made available given that the UQ plot indicates the estimates are quite accurate.

7 Conclusion

We have introduced a new Bayesian model for low-rank matrices when we have incomplete observations. Compared to prior Bayesian models for low-rank matrices such as BPFM, a distinct feature of our proposed BayesSMG introduces priors for low-rank subspaces considering the basis are orthonormal (thus, they are distributed on Stiefel manifolds). We also present an efficient sampling and inference method for BayesSMG. Besides achieving precise uncertainty quantification, the BayesSMG also enjoys nice statistical interpretation by drawing a

connection with subspace coherence. We demonstrate the good performance of BayesSMG using numerical experiments on synthetic and real data and real-world seismic sensors networks.

Acknowledgment

Henry Shaowu Yuchi and Yao Xie are supported by NSF CCF-1650913, NSF DMS-1938106, and NSF DMS-1830210. Simon Mak is supported by NSF CSSI Frameworks grant 2004571.

References

- Alquier, P., Cottet, V., Chopin, N., and Rousseau, J. (2014). Bayesian matrix completion: prior specification. *arXiv preprint arXiv:1406.1440*.
- Babacan, S. D., Luessi, M., Molina, R., and Katsaggelos, A. K. (2011). Low-rank matrix completion by variational sparse Bayesian learning. In *IEEE International Conference on Acoustics, Speech and Signal Processing (ICASSP)*, pages 2188–2191.
- Bensen, G., Ritzwoller, M., Barmin, M., Levshin, A. L., Lin, F., Moschetti, M., Shapiro, N., and Yang, Y. (2007). Processing seismic ambient noise data to obtain reliable broad-band surface wave dispersion measurements. *Geophysical journal international*, 169(3):1239–1260.
- Bertalmio, M., Sapiro, G., Caselles, V., and Ballester, C. (2000). Image inpainting. In *Proceedings of the 27th annual conference on Computer graphics and interactive techniques*, pages 417–424.
- Cai, J.-F., Candès, E. J., and Shen, Z. (2010). A singular value thresholding algorithm for matrix completion. *SIAM Journal on optimization*, 20(4):1956–1982.
- Calderbank, R., Thompson, A., and Xie, Y. (2015). On block coherence of frames. *Applied and Computational Harmonic Analysis*, 38(1):50 – 71.
- Candès, E. and Recht, B. (2009). Exact matrix completion via convex optimization. *Foundations of Computational Mathematics*, 9(6):717–772.
- Candès, E. J. and Plan, Y. (2010). Matrix completion with noise. *Proceedings of the IEEE*, 98(6):925–936.
- Candès, E. J. and Tao, T. (2010). The power of convex relaxation: Near-optimal

- matrix completion. *IEEE Transactions on Information Theory*, 56(5):2053–2080.
- Chen, Y., Fan, J., Ma, C., and Yan, Y. (2019). Inference and uncertainty quantification for noisy matrix completion. *Proceedings of the National Academy of Sciences*, 116(46):22931–22937.
- Chi, Y., Lu, Y. M., and Chen, Y. (2019). Nonconvex optimization meets low-rank matrix factorization: An overview. *IEEE Transactions on Signal Processing*, 67(20):5239–5269.
- Chikuse, Y. (2012). *Statistics on Special Manifolds*. Springer Science & Business Media.
- Davenport, M. A. and Romberg, J. (2016). An overview of low-rank matrix recovery from incomplete observations. *IEEE Journal of Selected Topics in Signal Processing*, 10(4):608–622.
- Dey, D. K., Liu, J., et al. (2007). A quantitative study of quantile based direct prior elicitation from expert opinion. *Bayesian Analysis*, 2(1):137–166.
- Fisher, N. I., Lewis, T., and Embleton, B. J. (1993). *Statistical analysis of spherical data*. Cambridge university press.
- Gelman, A., Carlin, J. B., Stern, H. S., Dunson, D. B., Vehtari, A., and Rubin, D. B. (2014). *Bayesian Data Analysis*, volume 2. CRC Press.
- Gelman, A. and Rubin, D. B. (1992). Inference from iterative simulation using multiple sequences. *Statistical Science*, 7(4):457–472.
- Gupta, A. K. and Nagar, D. K. (1999). *Matrix Variate Distributions*. CRC Press.
- Hoff, P. D. (2009). Simulation of the matrix Bingham–von Mises–Fisher distribution, with applications to multivariate and relational data. *Journal of Computational and Graphical Statistics*, 18(2):438–456.
- Hoffman, K. and Kunze, R. (1971). *Linear Algebra*. Englewood Cliffs, New Jersey.
- Jauch, M., Hoff, P. D., and Dunson, D. B. (2020). Monte carlo simulation on the stiefel manifold via polar expansion. *Journal of Computational and Graphical Statistics*, pages 1–23.
- Keshavan, R. H., Montanari, A., and Oh, S. (2010). Matrix completion from a few entries. *IEEE Transactions on Information Theory*, 56(6):2980–2998.
- Koltchinskii, V., Lounici, K., Tsybakov, A. B., et al. (2011). Nuclear-norm penalization and optimal rates for noisy low-rank matrix completion. *The Annals of Statistics*, 39(5):2302–2329.
- Lawrence, N. D. and Urtasun, R. (2009). Non-linear matrix factorization with

- Gaussian processes. In *Proceedings of the 26th International Conference on Machine Learning (ICML)*, pages 601–608.
- Negahban, S. and Wainwright, M. J. (2012). Restricted strong convexity and weighted matrix completion: Optimal bounds with noise. *Journal of Machine Learning Research*, 13(1):1665–1697.
- Recht, B. (2011). A simpler approach to matrix completion. *Journal of Machine Learning Research*, 12:3413–3430.
- Salakhutdinov, R. and Mnih, A. (2008). Bayesian probabilistic matrix factorization using Markov chain Monte Carlo. In *Proceedings of the 25th International Conference on Machine Learning (ICML)*, pages 880–887.
- Shen, J. (2001). On the singular values of Gaussian random matrices. *Linear Algebra and its Applications*, 326(1-3):1–14.
- Smith, R. C. (2013). *Uncertainty Quantification: Theory, Implementation, and Applications*. SIAM.
- Wang, Z. and Zhou, H. (2009). A general method of prior elicitation in bayesian reliability analysis. In *2009 8th International Conference on Reliability, Maintainability and Safety*, pages 415–419. IEEE.
- Xie, Y., Huang, J., and Willett, R. (2012). Change-point detection for high-dimensional time series with missing data. *IEEE Journal of Selected Topics in Signal Processing*, 7(1):12–27.
- Xu, D., Song, B., Xie, Y., Wu, S.-M., Lin, F.-C., and Song, W. (2019). Low-rank matrix completion for distributed ambient noise imaging systems. In *2019 53rd Asilomar Conference on Signals, Systems, and Computers*, pages 1059–1065. IEEE.
- Xue, H., Zhang, S., and Cai, D. (2017). Depth image inpainting: Improving low rank matrix completion with low gradient regularization. *IEEE Transactions on Image Processing*, 26(9):4311–4320.
- Zhou, M., Wang, C., Chen, M., Paisley, J., Dunson, D., and Carin, L. (2010). Nonparametric bayesian matrix completion. In *2010 IEEE Sensor Array and Multichannel Signal Processing Workshop*, pages 213–216. IEEE.
- Zou, H. and Hastie, T. (2005). Regularization and variable selection via the elastic net. *Journal of the Royal Statistical Society, Series B*, 67(2):301–320.

A Proofs

A.1 Proof of Lemma 2

Proof. We first prove part (a) of the lemma. To show that $\mathbf{X} \in \mathcal{T}$ almost surely, let \mathbf{Z} be an arbitrary matrix in $\mathbb{R}^{m_1 \times m_2}$, with SVD $\mathbf{Z} = \tilde{\mathbf{U}}\mathbf{D}\tilde{\mathbf{V}}^T$, $\mathbf{D} = \text{diag}(\{d_k\}_{k=1}^R)$. Letting $\mathbf{u}_k = \mathcal{P}_{\mathcal{U}}\tilde{\mathbf{u}}_k$ and $\mathbf{v}_k = \mathcal{P}_{\mathcal{V}}\tilde{\mathbf{v}}_k$, where $\tilde{\mathbf{u}}_k$ and $\tilde{\mathbf{v}}_k$ are column vectors for $\tilde{\mathbf{U}}$ and $\tilde{\mathbf{V}}$ respectively, we have $\mathbf{u}_k \in \mathcal{U}$ and $\mathbf{v}_k \in \mathcal{V}$ for $k = 1, \dots, R$. From Definition 1, \mathbf{X} can then be written as $\mathbf{X} = \mathcal{P}_{\mathcal{U}}\mathbf{Z}\mathcal{P}_{\mathcal{V}} = (\mathcal{P}_{\mathcal{U}}\tilde{\mathbf{U}})\mathbf{D}(\mathcal{P}_{\mathcal{V}}\tilde{\mathbf{V}})^T = \sum_{k=1}^R d_k \mathbf{u}_k \mathbf{v}_k^T$, as desired. Next, note that the pseudo-inverse of $\mathcal{P}_{\mathbf{u}}$, $(\mathcal{P}_{\mathbf{u}})^+$, is simply $\mathcal{P}_{\mathbf{u}}$, since $\mathcal{P}_{\mathbf{u}}(\mathcal{P}_{\mathbf{u}})^+\mathcal{P}_{\mathbf{u}} = (\mathcal{P}_{\mathbf{u}})^+\mathcal{P}_{\mathbf{u}}(\mathcal{P}_{\mathbf{u}})^+ = \mathcal{P}_{\mathbf{u}}$ by the idempotency of $\mathcal{P}_{\mathbf{u}}$, and $\mathcal{P}_{\mathbf{u}}(\mathcal{P}_{\mathbf{u}})^+ = (\mathcal{P}_{\mathbf{u}})^+\mathcal{P}_{\mathbf{u}}$ are both symmetric. Moreover, letting \det^* be the pseudo-determinant operator, we have $\det^*(\mathcal{P}_{\mathcal{U}}) = \det^*(\mathbf{U}\mathbf{U}^T) = \det(\mathbf{U}^T\mathbf{U}) = 1$, and $\det^*(\mathcal{P}_{\mathcal{V}}) = 1$ by the same argument. Using this along with Theorem 2.2.1 in Gupta and Nagar (1999), the density function $f(\mathbf{X})$ and the distribution of $\text{vec}(\mathbf{X})$ follow immediately.

We now prove part (b) of the lemma. From part (a), we have $\text{vec}(\mathbf{X}) \sim \mathcal{N}\{\mathbf{0}, \sigma^2(\mathcal{P}_{\mathcal{V}} \otimes \mathcal{P}_{\mathcal{U}})\}$, so:

$$[\mathbf{Y}_{\Omega}, \mathbf{X}_{\Omega^c}] \sim \mathcal{N} \left\{ \mathbf{0}, \begin{bmatrix} \sigma^2 \mathbf{R}_N(\Omega) + \eta^2 \mathbf{I} & \sigma^2(\mathcal{P}_{\mathcal{V}} \otimes \mathcal{P}_{\mathcal{U}})_{\Omega, \Omega^c} \\ \sigma^2(\mathcal{P}_{\mathcal{V}} \otimes \mathcal{P}_{\mathcal{U}})_{\Omega, \Omega^c}^T & \sigma^2(\mathcal{P}_{\mathcal{V}} \otimes \mathcal{P}_{\mathcal{U}})_{\Omega^c} \end{bmatrix} \right\}.$$

The expressions for $\mathbf{X}_{\Omega^c}^P$ and $\Sigma_{\Omega^c}^P$ in (4) then follow from the conditional density of the multivariate Gaussian distribution. Part (c) of the lemma can be shown in a similar way as for part (b). \square

A.2 Proof of Proposition 3

Proof. For fixed $\mathcal{P}_{\mathcal{U}}$ and $\mathcal{P}_{\mathcal{V}}$, \mathbf{X} can be written as:

$$\mathbf{X} = \mathcal{P}_{\mathcal{U}}\mathbf{Z}\mathcal{P}_{\mathcal{V}} = \mathbf{U}(\mathbf{U}^T\mathbf{Z}\mathbf{V})\mathbf{V}^T, \quad (17)$$

where $Z_{i,j} \stackrel{i.i.d.}{\sim} \mathcal{N}(0, \sigma^2)$, $\mathcal{P}_{\mathcal{U}} = \mathbf{U}\mathbf{U}^T$ and $\mathcal{P}_{\mathcal{V}} = \mathbf{V}\mathbf{V}^T$. By Theorem 2.3.10 in Gupta and Nagar (1999), each entry of $\tilde{\mathbf{Z}} = \mathbf{U}^T\mathbf{Z}\mathbf{V} \in \mathbb{R}^{R \times R}$ follows $\tilde{Z}_{i,j} \stackrel{i.i.d.}{\sim} \mathcal{N}(0, \sigma^2)$. Note that the distribution of $\tilde{\mathbf{Z}}$ is independent of the initial choice of $\mathcal{P}_{\mathcal{U}}$ and $\mathcal{P}_{\mathcal{V}}$ (and thereby \mathbf{U} and \mathbf{V}). By Theorem 1 of Shen (2001), $\tilde{\mathbf{Z}}$ can be further factorized via its SVD:

$$\tilde{\mathbf{Z}} = \tilde{\mathbf{U}}\mathbf{D}\tilde{\mathbf{V}}^T, \quad (18)$$

with independent $\tilde{\mathbf{U}} \sim U(\mathcal{V}_{R,R})$, $\tilde{\mathbf{V}} \sim U(\mathcal{V}_{R,R})$ and $\text{diag}(\mathbf{D})$ following the repulsed normal distribution (7).

Next, assign independent uniform priors $U(\mathcal{G}_{R,m_1-R})$ and $U(\mathcal{G}_{R,m_2-R})$ on projection matrices $\mathcal{P}_{\mathcal{U}}$ and $\mathcal{P}_{\mathcal{V}}$, which induces independent uniform priors $U(\mathcal{V}_{R,m_1-R})$ and $U(\mathcal{V}_{R,m_2-R})$ on frames \mathbf{U} and \mathbf{V} . From (17), we have:

$$\mathbf{X} = \mathbf{U}(\tilde{\mathbf{U}}\mathbf{D}\tilde{\mathbf{V}}^T)\mathbf{V}^T = (\mathbf{U}\tilde{\mathbf{U}})\mathbf{D}(\mathbf{V}\tilde{\mathbf{V}})^T =: \tilde{\mathbf{U}}\mathbf{D}\tilde{\mathbf{V}}^T. \quad (19)$$

Note that $\tilde{\tilde{\mathbf{U}}} = \mathbf{U}\tilde{\mathbf{U}}$ is an orthonormal frame, since $(\mathbf{U}\tilde{\mathbf{U}})^T(\mathbf{U}\tilde{\mathbf{U}}) = \tilde{\mathbf{U}}^T(\mathbf{U}^T\mathbf{U})\tilde{\mathbf{U}} = \tilde{\mathbf{U}}^T\tilde{\mathbf{U}} = \mathbf{I}$. Moreover, $\tilde{\tilde{\mathbf{U}}} \sim U(\mathcal{V}_{R,m_1-R})$, since \mathbf{U} and $\tilde{\mathbf{U}}$ are independent and uniformly distributed. Similarly, one can show $\tilde{\tilde{\mathbf{V}}} = \mathbf{V}\tilde{\mathbf{V}} \sim U(\mathcal{V}_{R,m_2-R})$ as well, which proves the proposition. \square

A.3 Proof of Lemma 4

Proof. Since $U(\mathcal{G}_{R,m-R})$ is a special case of the matrix Langevin distribution (Section 2.3.2 in Chikuse (2012)), it follows from (2.3.22) of Chikuse (2012) that $[\mathcal{P}_{\mathcal{U}}|R] \propto 1$ and $[\mathcal{P}_{\mathcal{V}}|R] \propto 1$. For fixed η^2 and σ^2 , the MAP estimator for \mathbf{X} then becomes:

$$\begin{aligned} \tilde{\mathbf{X}} &\in \underset{\mathbf{X} \in \mathbb{R}^{m_1 \times m_2}}{\text{Argmax}} [\mathbf{Y}_{\Omega}|\mathbf{X}, \eta^2][\mathbf{X}|\mathcal{P}_{\mathcal{U}}, \mathcal{P}_{\mathcal{V}}, \sigma^2, R] \cdot \\ &\quad [\mathcal{P}_{\mathcal{U}}|R][\mathcal{P}_{\mathcal{V}}|R][R] \\ &\quad \text{s.t. } \mathcal{P}_{\mathcal{U}} \in \mathcal{G}_{R,m_1-R}, \mathcal{P}_{\mathcal{V}} \in \mathcal{G}_{R,m_2-R}, R \leq m_1 \wedge m_2 \\ &\in \underset{\mathbf{X} \in \mathbb{R}^{m_1 \times m_2}}{\text{Argmax}} \exp \left\{ -\frac{1}{2\eta^2} \|\mathbf{Y}_{\Omega} - \mathbf{X}_{\Omega}\|_2^2 \right\} \cdot \\ &\quad \left[\frac{1}{(2\pi\sigma^2)^{R^2/2}} \exp \left\{ -\frac{1}{2\sigma^2} \text{tr} [(\mathbf{X}\mathcal{P}_{\mathcal{V}})^T(\mathcal{P}_{\mathcal{U}}\mathbf{X})] \right\} \right] \cdot \\ &\quad \text{s.t. } \mathcal{P}_{\mathcal{U}} \in \mathcal{G}_{R,m_1-R}, \mathcal{P}_{\mathcal{V}} \in \mathcal{G}_{R,m_2-R}, R \leq m_1 \wedge m_2 \\ &\in \underset{\mathbf{X} \in \mathbb{R}^{m_1 \times m_2}}{\text{Argmin}} \left[\frac{1}{\eta^2} \|\mathbf{Y}_{\Omega} - \mathbf{X}_{\Omega}\|_2^2 + \log(2\pi\sigma^2)R^2 + \right. \\ &\quad \left. \frac{1}{\sigma^2} \text{tr} [(\mathbf{X}\mathcal{P}_{\mathcal{V}})^T(\mathcal{P}_{\mathcal{U}}\mathbf{X})] \right] \\ &\quad \text{s.t. } \mathcal{P}_{\mathcal{U}} \in \mathcal{G}_{R,m_1-R}, \mathcal{P}_{\mathcal{V}} \in \mathcal{G}_{R,m_2-R}, R \leq m_1 \wedge m_2. \end{aligned}$$

Since $\mathbf{X} = \mathcal{P}_{\mathcal{U}}\mathbf{Z}\mathcal{P}_{\mathcal{V}}$, we have $\mathbf{X} = \mathbf{U}\mathbf{D}\mathbf{V}^T$ for some $\mathbf{D} = \text{diag}(\{d_k\}_{k=1}^R)$, $\mathbf{U} \in \mathbb{R}^{m_1 \times R}$ and $\mathbf{V} \in \mathbb{R}^{m_2 \times R}$, where \mathbf{U} and \mathbf{V} are R -frames satisfying $\mathcal{P}_{\mathcal{U}} = \mathbf{U}\mathbf{U}^T$

and $\mathcal{P}_{\mathcal{V}} = \mathbf{V}\mathbf{V}^T$. Hence:

$$\begin{aligned}
& \text{tr} [(\mathbf{X}\mathcal{P}_{\mathbf{V}})^T(\mathcal{P}_{\mathbf{U}}\mathbf{X})] \\
&= \text{tr} [(\mathbf{V}\mathbf{V}^T)(\mathbf{V}\mathbf{D}\mathbf{U}^T)(\mathbf{U}\mathbf{U}^T)(\mathbf{U}\mathbf{D}\mathbf{V}^T)] \\
&= \text{tr} [(\mathbf{V}^T\mathbf{V})^2\mathbf{D}(\mathbf{U}^T\mathbf{U})^2\mathbf{D}] && (\text{cyclic invariance of trace}) \\
&= \text{tr} [\mathbf{D}^2] && (\mathbf{V}^T\mathbf{V} = \mathbf{I} \text{ and } \mathbf{U}^T\mathbf{U} = \mathbf{I}) \\
&= \|\mathbf{X}\|_F^2, && (\text{Frob. norm is equal to Schatten 2-norm})
\end{aligned}$$

which proves the expression in (11). \square

A.4 Proof of Theorem 7

Proof. Consider the following block decomposition:

$$\mathbf{R}_{N+1}(\Omega \cup (i, j)) + \gamma^2 \mathbf{I} = \begin{pmatrix} \mathbf{R}_N(\Omega) + \gamma^2 \mathbf{I} & \boldsymbol{\nu}_i(\mathcal{U}) \circ \boldsymbol{\nu}_j(\mathcal{V}) \\ [\boldsymbol{\nu}_i(\mathcal{U}) \circ \boldsymbol{\nu}_j(\mathcal{V})]^T & \mu_i(\mathcal{U})\mu_j(\mathcal{V}) + \gamma^2 \end{pmatrix}.$$

Using the Schur complement identity for matrix inverses Hoffman and Kunze (1971), we have:

$$[\mathbf{R}_{N+1}(\Omega \cup (i, j)) + \gamma^2 \mathbf{I}]^{-1} = \begin{pmatrix} \boldsymbol{\Gamma} + \tau^{-1}\boldsymbol{\Gamma}\boldsymbol{\xi}\boldsymbol{\xi}^T\boldsymbol{\Gamma} & -\tau^{-1}\boldsymbol{\xi}^T\boldsymbol{\Gamma} \\ -\tau^{-1}\boldsymbol{\Gamma}\boldsymbol{\xi} & \tau^{-1} \end{pmatrix}, \quad (20)$$

where $\boldsymbol{\xi} = \boldsymbol{\nu}_i(\mathcal{U}) \circ \boldsymbol{\nu}_j(\mathcal{V})$, $\boldsymbol{\Gamma} = [\mathbf{R}_N(\Omega) + \gamma^2 \mathbf{I}]^{-1}$ and $\tau = \mu_i(\mathcal{U})\mu_j(\mathcal{V}) - \boldsymbol{\xi}^T\boldsymbol{\Gamma}\boldsymbol{\xi} + \gamma^2$. Using the conditional variance expression in (15), $\tau = \text{Var}(X_{i,j}|\mathbf{Y}_{\Omega})/\sigma^2 + \gamma^2$. Letting $\tilde{\boldsymbol{\xi}} = \boldsymbol{\nu}_k(\mathcal{U}) \circ \boldsymbol{\nu}_l(\mathcal{V})$ and applying (15) again, it follows that:

$$\begin{aligned}
& \text{Var}(X_{k,l}|\mathbf{Y}_{\Omega \cup (i,j)}) \\
&= \sigma^2 \left\{ \mu_k(\mathcal{U})\mu_l(\mathcal{V}) - \tilde{\boldsymbol{\xi}}^T \boldsymbol{\Gamma} \tilde{\boldsymbol{\xi}} \right\} \\
&\quad - \tau^{-1} \sigma^2 \left\{ \boldsymbol{\nu}_{i,j}^T [\mathbf{R}_N(\Omega) + \gamma^2 \mathbf{I}]^{-1} \boldsymbol{\nu}_{k,l} - \nu_{i,k}(\mathcal{U})\nu_{j,l}(\mathcal{V}) \right\}^2 \\
&\quad \quad \quad (\text{using (20) and algebraic manipulations}) \\
&= \text{Var}(X_{k,l}|\mathbf{Y}_{\Omega}) - \frac{\text{Cov}^2(X_{i,j}, X_{k,l}|\mathbf{Y}_{\Omega})}{\text{Var}(X_{i,j}|\mathbf{Y}_{\Omega}) + \eta^2}, \quad (\text{from (4)})
\end{aligned}$$

which proves the theorem. \square

A.5 Proof of Corollary 1

Proof. This follows directly from Theorem 7 and the fact that:

$$\text{Cov}^2(X_{i,j}, X_{k,l} | \mathbf{Y}_{\Omega_{1:N}}) / \{\text{Var}(X_{i,j} | \mathbf{Y}_{\Omega_{1:N}}) + \eta^2\} > 0.$$

□

A.6 Proof of full conditional distributions

Proof. For fixed rank R , the posterior distribution $[\Theta | \mathbf{Y}]$ can be written as:

$$\begin{aligned} [\mathbf{U}, \mathbf{D}, \mathbf{V}, \sigma^2 | \mathbf{Y}] &\propto [\mathbf{Y} | \mathbf{U}, \mathbf{D}, \mathbf{V}, \sigma^2] \cdot [\mathbf{U}] \cdot [\mathbf{V}] \cdot [\mathbf{D} | \sigma^2] \cdot [\sigma^2] \\ &\propto \frac{1}{(\eta^2)^{(m_1 m_2)/2}} \exp \left\{ -\frac{1}{2\eta^2} \|\mathbf{Y} - \mathbf{U} \mathbf{D} \mathbf{V}^T\|_F^2 \right\} \cdot \frac{1}{(\sigma^2)^{R/2}} \\ &\quad \cdot \exp \left\{ -\frac{1}{2\sigma^2} \sum_{k=1}^R d_k^2 \right\} \cdot \prod_{\substack{k,l=1 \\ k < l}}^R |d_k^2 - d_l^2| \\ &\quad \cdot \frac{1}{(\sigma^2)^{\alpha_{\sigma^2}+1}} \exp \left\{ -\frac{\beta_{\sigma^2}}{\sigma^2} \right\} \cdot \frac{1}{(\eta^2)^{\alpha_{\eta^2}+1}} \exp \left\{ -\frac{\beta_{\eta^2}}{\eta^2} \right\}. \end{aligned}$$

From this, the full conditional distributions can then be derived as follows:

$$\begin{aligned} [\mathbf{U} | \mathbf{Y}, \mathbf{D}, \mathbf{V}, \sigma^2, \eta^2] &\propto \text{etr}\{(\mathbf{Y} \mathbf{V} \mathbf{D})^T \mathbf{U} / \eta^2\} \sim vMF(m_1, R, \mathbf{Y} \mathbf{V} \mathbf{D} / \eta^2), \\ [\mathbf{V} | \mathbf{Y}, \mathbf{U}, \mathbf{D}, \sigma^2, \eta^2] &\propto \text{etr}\{(\mathbf{Y}^T \mathbf{U} \mathbf{D})^T \mathbf{V} / \eta^2\} \sim vMF(m_2, R, \mathbf{Y}^T \mathbf{U} \mathbf{D} / \eta^2), \\ [\mathbf{D} | \mathbf{Y}, \mathbf{U}, \mathbf{V}, \sigma^2, \eta^2] &\propto \exp \left\{ -\frac{1}{2\eta^2} \|\mathbf{Y} - \mathbf{U} \mathbf{D} \mathbf{V}^T\|_F^2 \right\} \exp \left\{ -\frac{1}{2\sigma^2} \sum_{k=1}^R d_k^2 \right\} \prod_{\substack{k,l=1 \\ k < l}}^R |d_k^2 - d_l^2| \\ &\sim \mathcal{RN}(\sigma^2 \text{diag}(\mathbf{U}^T \mathbf{Y} \mathbf{V}) / (\eta^2 + \sigma^2), \eta^2 \sigma^2 / (\eta^2 + \sigma^2)) \\ [\sigma^2 | \mathbf{Y}, \mathbf{U}, \mathbf{D}, \mathbf{V}, \eta^2] &\sim IG(\alpha + R/2, \beta + \text{tr}(\mathbf{D}^2)/2) \\ [\eta^2 | \mathbf{Y}, \mathbf{U}, \mathbf{D}, \mathbf{V}, \sigma^2] &\sim IG(\alpha_{\eta^2} + m_1 m_2 / 2, \beta_{\eta^2} + \|\mathbf{Y} - \mathbf{U} \mathbf{D} \mathbf{V}^T\|_F^2 / 2). \end{aligned}$$

□